Flow in Rough Self-Affine Fractures Joints

José S. Andrade Jr.* and Ascânio D. Araújo

Departamento de Física, Universidade Federal do Ceará, 60451-970 Fortaleza, Ceará, Brazil

Fernando A. Oliveira

*International Center of Condensed Matter Physics and Instituto de Física,
Universidade de Brasília, CP 04667, 70919-970 Brasília DF, Brazil*

Alex Hansen

Department of Physics, Norwegian University of Science and Technology, N–7491 Trondheim, Norway
(Dated: February 4, 2008)

We investigate viscous and non-viscous flow in two-dimensional self-affine fracture joints through direct numerical simulations of the Navier-Stokes equations. As a novel hydrodynamic feature of this flow system, we find that the effective permeability at higher Reynolds number to cubic order, falls into two regimes as a function of the Hurst exponent h characterizing the fracture joints. For $h > 1/2$, we find a weak dependency whereas for $h < 1/2$, the dependency is strong. A similar behavior is found for the higher order coefficients. We also study the velocity fluctuations in space of a passive scalar. These are strongly correlated on smaller length scales, but decorrelates on larger scales. Moreover, the fluctuations on larger scale are insensitive to the value of the Reynolds number.

PACS numbers: 47.53.+n, 47.56.+r, 47.60.+i, 83.50.-v

The transport of oil in carbonate reservoirs is dominated by flow through internal fractures. As about 10-15% of the world's known reservoirs consist of carbonates and that these contain about 50% of the remaining oil, it is surprising that this problem has received so little attention as it has from not only the physics community, but also the engineering communities. It is not uniquely from a practical, economical point of view that this is a worthwhile problem to study. The progress made in fracture morphology over the last years, has uncovered a large number of basic questions to be answered, and the present problem is one of these. It has become increasingly clear that the morphology of brittle fractures follows certain scaling laws first observed in the mid-eighties [1], demonstrating that such surfaces are *self-affine.* That is, by rescaling the in-plane length scale x by λx requires the out-of-plane scale y to be rescaled by $\lambda^h y$ for the fracture surface to remain statistically unchanged, with h being the roughness exponent. In the early nineties, it was suggested that h is universal and has a value of 0.8 [2]. There is today some evidence that other values of the Hurst exponent may occur depending on the material and how the fracture has been produced [3], thus suggesting more than one universality class.

For single-phase fluid flow in porous media and fractures, it is common to characterize the system in terms of Darcy's law [4, 5], which assumes that a *global* index, the permeability k, relates the average fluid velocity V with the pressure drop ΔP across the system, $V = -k\Delta P/\mu L$. Here L is the length of the sample in the flow direction and μ is the viscosity of the fluid. However, in order to

understand the interplay between porous structure and fluid flow, it is necessary to examine *local* aspects of the pore space morphology and relate them to the relevant mechanisms of momentum transfer (viscous and inertial forces). Flow in self-affine faults was to our knowledge first discussed by Roux *et al.* [6], where they considered a fracture fault consisting of two matching walls that have been moved along the fracture plane with respect to each other. If the in-plane movement is x, then – due to the self-affinity of the fault – the amplitude of the fault will be proportional to x^h. It was claimed in [6] that the permeability of a two-dimensional fracture fault would scale as x^{2h}, based on using the self-affinity to determine the scaling properties of an effective channel width. However, numerical studies by Gutfraind *et al.* [7] using
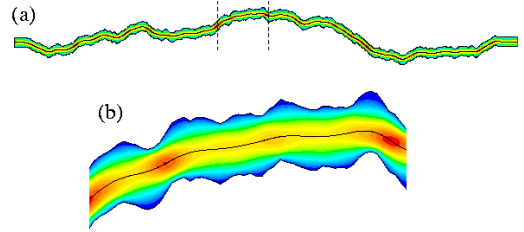

FIG. 1: (a) Contour plot of the local velocity magnitude along a typical realization of the self-affine rough channel ($h = 0.8$) subjected to low Reynolds conditions. Fluid is pushed from left to right. The colors ranging from blue to red correspond to low and high velocity magnitudes, respectively. The solid line in the center of the channel corresponds to the streamline that divides the flux into two equal parts. The zoom shown in (b) reveals the presence of high velocity spots in the flow field induced by the occurrence of high slopes in the channel geometry.
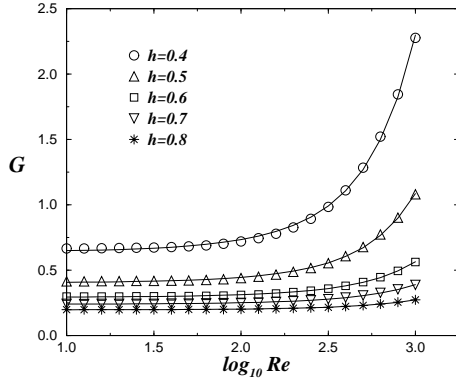
*Electronic address: soares@fisica.ufc.br

FIG. 2: Dependence of the hydraulic resistance $G \equiv -\Delta P w^2/\mu V L$ on the Reynolds number for different values of the roughness exponent h. In all cases, the plateau corresponding to Darcy's law (constant G) is followed by a nonlinear regime that reflects the effect of convection on the flow. The error bars are smaller than the symbols and the solid lines are the best fit to the data of Eq. (4).

FIG. 3: (a) Variation of the parameter α as in Eq. (4 with the exponent h characterizing the roughness of the channel geometry. The two dashed lines correspond to different regimes dictated by the nature of the correlations. The crossover at $h \approx 0.5$ delimits anti-correlated ($h < 0.5$) and correlated ($h > 0.5$) signals. The inset shows that the parameters β and γ of Eq. (4) behave in a very similar way.

lattice gas methods, demonstrated that the permeability should be controlled by the narrowest neck in the system. In a subsequent work [8], the permeability of self-affine rough fractures with wide and narrow apertures has been investigated analytically and confirmed through numerical simulations with the lattice Boltzmann method. The flow in self-affine fracture *joints*, where the two matching fractures are moved apart by a distance w but without any relative movement in fracture plane ($x = 0$), has been previously studied by Skjetne *et al.* [9].

Strictly speaking, the concept of permeability as a global index for flow in fractures should be restricted to viscous flow (linear) conditions. More precisely, Darcy's law should only be applicable for flow at sufficiently low Reynolds number, defined here as $Re \equiv \rho V w/\mu$, where w is the fracture opening. It is well known, however, that the role of inertial forces (convection) to flow in disordered media should be examined in the framework of the laminar flow regime, before assuming that fully developed turbulence effects are already present [4, 10, 11]. Much less effort has been dedicated to address this problem in the specific context of flow through rough fractures. For instance, the computational fluid dynamics simulations presented in Ref. [9] indicate that vanishing weak and strong inertial flows can be quantitatively described in different ways, namely the Darcy, weak inertia and Forchheimer empirical equations, respectively. Here we investigate by direct simulation of the Navier-Stokes equations the departure from Darcy's law in laminar flow through self-affine fracture joints. We confirm that the physical description underlying a classical cubic equation provides a legitimate correlation for the flow in the fracture over a wide range of Reynolds number conditions. We then demonstrate that it is also possible to characterize this transition from linear to nonlinear behavior in terms of the spatial correlations in the fluid velocity.
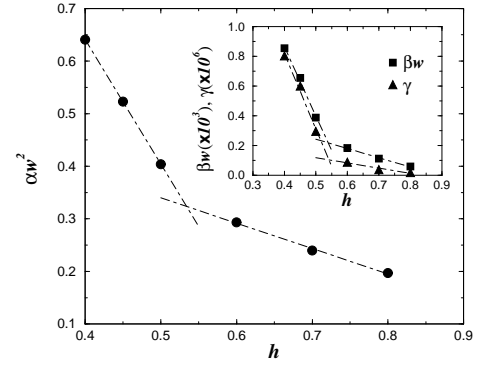
This allows us to elucidate certain characteristics of the fluid flow phenomenon in fracture fault geometries that have not been studied before.

The self-affine surfaces are generated here with a Fourier method [12] for which we specify the length N and width m, both in terms of the number of nodes, and the roughness exponent h. The surface is given by y_i (measured in units of the lattice constant), and $m = \max y_i - \min y_i$. Since the lattice constant is δ, the length of the system is $L = N\delta$ and its amplitude is given by $a = m\delta$. When L is to be changed while δ is to be kept fixed, we scale $N \to \lambda N$ and $m \to \lambda m$. On the other hand, when δ is to be changed, while L is to be kept fixed, we let $N \to \lambda N$ and keep m fixed. The fracture opening w is kept fixed.

The mathematical description for the fluid mechanics in the interstitial porous space is based on the assumptions that we have a continuum, Newtonian and incompressible fluid flowing under steady state conditions. Thus, the Navier-Stokes and continuity equations reduce to

$$\rho\, \mathbf{u} \cdot \nabla \mathbf{u} = -\nabla p + \mu\, \nabla^2 \mathbf{u}\,, \qquad (1)$$

$$\nabla \cdot \mathbf{u} = 0\,, \qquad (2)$$

where $\mathbf{u}$ and p are the local velocity and pressure fields, respectively, and ρ is the density of the fluid. In our simulations, we consider non-slip boundary conditions along the entire solid-fluid interface. In addition, the changes in velocity rates are assumed to be zero at the exit $x = L$ (gradientless boundary conditions), whereas a uniform velocity profile, $u_x(0, y) = V$ and $u_y(0, y) = 0$, is imposed at the inlet of the channel.

The numerical solution of Eqs. (1) and (2) for the velocity and pressure fields in the pore space is obtained

through discretization by means of the control volume finite-difference technique [13]. Considering the complex geometries involved, we build an unstructured mesh of triangular grid elements based on a Delaunay network. For the largest fracture investigated, namely $L = 512$, around 10^6 cells are necessary to generate satisfactory results when compared with numerical meshes of larger resolution. The convergence criteria used in the simulations are defined in terms of residuals, i.e., the degree up to which the conservation equations are satisfied throughout the flow field. In all our simulations, convergence is considered to be achieved only when each of the residuals falls below 10^{-6}.

In Fig. 1 we show the contour plot of the velocity magnitude in a typical self-affine channel under viscous flow conditions, i.e., at very low Reynolds number ($Re = 10$). Clearly, the spots of high velocity correspond to those regions with high slopes in the channel due to their reduced effective areas for flow, namely the cross-sections orthogonal to the walls. Also shown in Fig. 1 is the streamline that divides the flow exactly into two zones of equal flux. As discussed later, this line will be adopted here as a reference location to study the spatial correlations in the local fluid velocity for different Reynolds conditions.

The approach we adopt here to macroscopically characterize the effect of convection on flow through the self-affine channel is to employ the cubic relation

$$-\frac{\Delta P}{L} = \alpha \mu V + \beta \rho V^2 + \frac{\gamma \rho^2 V^3}{\mu} \; , \qquad (3)$$

where the coefficient α corresponds to the reciprocal of the permeability of the porous material and the two remaining terms containing β and γ can be interpreted, respectively, as second and third order corrections that should account for the contribution of inertial forces in the fluid flow. At sufficiently low Reynolds, Eq. (3) reduces to Darcy's law. Rewriting (3) in terms of the Reynolds number we obtain,

$$G = \alpha w^2 + \beta w Re + \gamma Re^2 \; , \qquad (4)$$

with $G \equiv -\Delta P w^2 / \mu V L$ being a dimensionless measure of the *hydraulic resistance*. Fig. 2 shows the results of our flow simulations in terms of the variables G and Re for different values of the roughness exponent h. After computing and averaging G over a total of 10 realizations for each value of h and a wide range of Reynolds numbers, we fit the results with Eq. (4) to estimate the coefficients α, β and γ. In agreement with real flow experiments, we observe a transition from constant G (Darcy's law) to nonlinear flow behavior at a value of Re that depends significantly on the roughness. As shown in Fig. 3, the coefficient α generally decreases with the roughness exponent h. There is, however, a clear crossover at a value of $h \approx 0.5$ separating two distinct regimes that characterize the influence of the channel geometry on the parameter α. Interestingly, the value $h = 0.5$ corresponds exactly to the transition point between anti-correlated ($h < 0.5$)
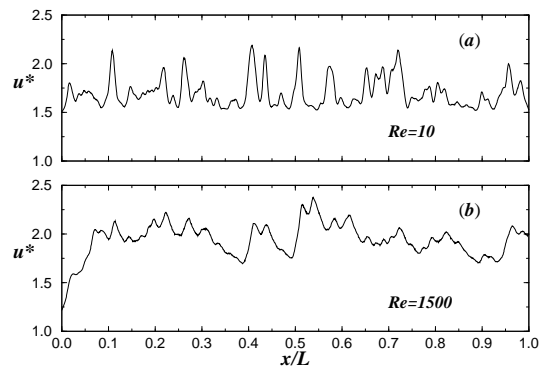

FIG. 4: (a) Profile of the velocity magnitude along the streamline located at the center of the rough channel (see Fig. 1) for a flow field calculated at low Reynolds conditions ($Re = 10$). (b) The same as in (a), but for $Re = 1500$.

and correlated ($h > 0.5$) self-affine interfaces [14]. To the best of our knowledge, this is the first time that a clear connection can be drawn in order to relate the degree of correlation in the interface geometry and the single-phase flow behavior through self-affine fractures. The results shown in the inset of Fig. 3 reveal that the coefficients β and γ also decrease with h and display similar crossovers between correlated and anti-correlated geometries.

Next we study the fluctuations in velocity of a massless particle (i.e., a passive tracer) released right at the center of the channel inlet. As mentioned earlier, this particle will then follow a trajectory that coincides with the streamline dividing the flow into two regions of equal flux (see Fig. 1). In Fig. 4, we show the variation of its normalized velocity magnitude $u^* = u/V$, along the main flow direction x in a typical realization of the rough channel and for two different values of the Reynolds number. At low Re (Fig. 4a), the location and intensity of the velocity peaks essentially correspond to the spatial variation in amplitude of the local slopes along the fracture. At high Re (Fig. 4b), the situation becomes quite different. Due to inertia, the effect on the flow field of the local channel geometry reveals a *persistent* behavior in the local velocity fluctuations, when compared to the results obtained at low Re (Fig. 4a). More precisely, whenever a sudden increase in velocity is observed due to the presence of a narrow constriction in the channel, the signal tends to decay more slowly at higher Re conditions, before the particle experiences another substantial amplitude fluctuation. It is interesting to note that the same sequence of peaks and valleys presented in Fig. 4a can also be observed in Fig. 4b, but with the difference that the background velocity is generally much higher at high Re values because of inertial effects.

Due to the interplay between flow and the self-affine characteristic of the fracture interfaces utilized here [14], one should expect the velocity profiles shown in Fig. 4 to contain a certain degree of correlation. More precisely, long-range power-law correlations in velocity magnitude
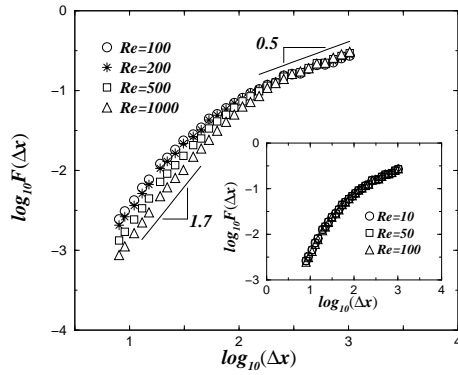
4

FIG. 5: (a) Logarithmic plot of the detrended fluctuation function $F(\Delta x)$ calculated from 10 realizations of velocity magnitude profiles (see Fig. 4) and four different values of the Reynolds number. The two straight lines show the best power law fits to the data in the scaling regions. The difference in the slopes indicates the passage from a highly correlated ($\zeta \approx 1.7$) to an uncorrelated ($\zeta \approx 0.5$) series. The inset shows that the function $F(\Delta x)$ is invariant with Re for $Re < 100$.

are identified and quantified here by means of the *detrended fluctuation analysis* (DFA) [15]. According to this method, one can avoid the spurious observation of long-range correlations due to non-stationarities by integrating the time series and mapping it to a self-affine stochastic process. The velocity profile $u^*(x)$ is integrated, after subtracting the overall velocity average, and divided into boxes of equal length Δx. The local linear trend is then calculated as the least-squares straight line that fits the data within each interval. The difference between the integrated time series and the local trend in each box gives the detrended time series, from which

we can compute the root-mean-square fluctuation $F(\Delta x)$ [15]. Scaling is present if $F(\Delta x)$ has a power-law dependence on Δx, $F(\Delta x) \simeq (\Delta x)^\zeta$, where the exponent ζ characterizes the nature of the long-range correlations.

The results in Fig. 5 show that, regardless of the Reynolds number, the function $F(\Delta x)$ displays a highly correlated power-law regime ($\zeta = 1.7 \pm 0.03$) at small length scales followed by a typically uncorrelated scaling ($\zeta = 0.5 \pm 0.01$) at larger values of the Δx window. The only difference is that, above a sufficiently high value of Re (see the inset of Fig. 5), the crossover from correlated to uncorrelated behavior starts to increase with Re. This is compatible with our previous qualitative analysis based on the simple inspection of the profiles in Fig. 4. The first (highly correlated) regime is a direct consequence of the channel self-affinity inducing long-range correlations in tracer velocity, where a large exponent denotes the fractional-Brownian aspect of the signal.

In summary, we have presented a numerical study of single-phase flow in self-affine fracture joints. We find that each of the coefficients α, β and γ, characterizing the cubic generalization of the Darcy equation (3) depends nearly linearly on the Hurst exponent h in two distinct regimes that meet at $h \approx 0.5$. We also follow a passive scalar particle released at the center of the channel, finding that its velocity fluctuations are characterized by strong spatial correlations on small scales, crossing over to uncorrelated random-walk-like behavior on larger scale. The large-scale behavior is insensitive to Re.

[1] B. B. Mandelbrot, D. E. Passoja, and A. J. Paullay, Nature **308**, 721 (1984); S. R. Brown and C. H. Scholz, J. Geophys. Res. **90**, 12575 (1985).

[2] E. Bouchaud, G. Lapasset, and J. Planés, Europhys. Lett. **13**, 73 (1990); K. J. Måløy, A. Hansen, E. L. Hinrichsen, and S. Roux, Phys. Rev. Lett. **68**, 213 (1992); J. Schmittbuhl, S. Gentier, and S. Roux, Geophys. Res. Lett. **20**, 639 (1993); B. L. Cox and J. S. Y. Wang, Fractals **1**, 87 (1993); J. Schmittbuhl, F. Schmitt, and C. H. Scholz, J. Geophys. Res. **100**, 5953 (1995).

[3] L. Ponson, D. Bonamy and E. Bouchaud, Phys. Rev. Lett. **96**, 035506 (2006).

[4] F. A. L. Dullien, *Porous Media - Fluid Transport and Pore Structure* (Academic, New York, 1979).

[5] M. Sahimi, *Applications of Percolation Theory* (Taylor & Francis, London, 1994); M. Sahimi, *Flow and Transport in Porous Media and Fractured Rock* (VCH, Boston, 1995).

[6] S. Roux, J. Schmittbuhl, J.-P. Vilotte and A. Hansen, Europhys. Lett. **23**, 277 (1993).

[7] R. Gutfraind and A. Hansen, Transp. Porous Media **18**,

131 (1995); R. Gutfraind, I. Ippolito and A. Hansen, Phys. Fluids **7**, 1938 (1995).

[8] G. Drazer and J. Koplik, Phys. Rev. E **62**, 8076 (2000).

[9] E. Skjetne, A. Hansen and J. S. Gudmundsson, J. Fluid Mech. **383**, 1 (1999).

[10] D. R. Koch and A. J. C. Ladd, J. Fluid Mech. **349**, 31 (1997).

[11] J. S. Andrade Jr., U. M. S. Costa, M. P. Almeida, H. A. Makse and H. E. Stanley, Phys. Rev. Lett. **82**, 5249 (1999).

[12] R. F. Voss in R. A. Earshaw, Ed. *Fundamental Algorithms for Computer Graphics* (Springer Verlag, Berlin, 1985).

[13] S. V. Patankar, *Numerical Heat Transfer and Fluid Flow* (Hemisphere, Washington DC, 1980); The FLUENT (trademark of FLUENT Inc.) fluid dynamics analysis package has been used in this study.

[14] *Fractals and Disordered Systems* 2nd ed., edited by A. Bunde and S. Havlin (Springer-Verlag, New York, 1996).

[15] C.-K. Peng, S. V. Buldyrev, S. Havlin, M. Simons, H. E. Stanley, and A. L. Goldberger, Phys. Rev. E **49**, 1685

(1994).